

# Treatment of the proton-proton Coulomb force in proton-deuteron breakup Faddeev calculations

H. Witała, R. Skibiński, and J. Golak

*M. Smoluchowski Institute of Physics,  
Jagiellonian University, PL-30059 Kraków, Poland*

W. Glöckle

*Institut für theoretische Physik II, Ruhr-Universität Bochum, D-44780 Bochum, Germany*

(Dated: November 11, 2018)

## Abstract

We extend our approach to incorporate the proton-proton (pp) Coulomb force into the three-nucleon (3N) Faddeev calculations from elastic proton-deuteron (pd) scattering to the breakup process. The main new ingredient is a 3-dimensional screened pp Coulomb t-matrix obtained by a numerical solution of the 3-dimensional Lippmann-Schwinger (LS) equation. We demonstrate numerically that the proton-deuteron (pd) breakup observables can be determined from the resulting on-shell 3N amplitudes increasing the screening radius. However, contrary to the pd elastic scattering, the screening limit exists only after renormalisation of the pp t-matrices.

PACS numbers: 21.45.-v, 21.45.Bc, 25.10.+s, 25.40.Cm

## I. INTRODUCTION

The long-range nature of the Coulomb force prevents the application of the standard techniques developed for short-range interactions in the analysis of nuclear reactions involving two protons. One proposal to avoid the difficulties including the Coulomb force is to use a screened Coulomb interaction and to reach the pure Coulomb limit through application of a renormalisation procedure [1, 2, 3, 4].

For elastic pd scattering first calculations, with modern nuclear forces and the Coulomb force included, have been achieved in a variational hyperspherical harmonic approach [5]. Only recently the inclusion of the Coulomb force was undertaken also for the pd breakup reaction [6]. In [6], contrary to [5] where the exact Coulomb force in coordinate representation has been used directly, a screened pp Coulomb force has been applied in momentum space and in a partial wave basis. In order to get the final predictions which can be compared to the data, the limit to the unscreened situation has been performed numerically applying a renormalization to the resulting 3N on-shell amplitudes [6, 7]. This allowed for the first time to analyze high-precision pd breakup data and provided a significant improvement of data description in cases where the Coulomb force plays an important role [8].

Recently we developed a novel approach to include the pp Coulomb force into the momentum space 3N Faddeev calculations [9]. It is based on a standard formulation for short range forces and relies on the screening of the long-range Coulomb interaction. In order to avoid all uncertainties connected with the application of the partial wave expansion, inadequate when working with long-range forces, we used directly the 3-dimensional pp screened Coulomb t-matrix. We demonstrated the feasibility of that approach in case of elastic pd scattering using a simple dynamical model for the nuclear part of the interaction. It turned out that the screening limit exists without the need of renormalisation not only for pd elastic scattering observables but for the elastic pd amplitude itself.

In spite of the substantial progress in the pd breakup treatment achieved in [6, 7] some important questions remained unanswered. One concerns directly the results of these calculations for two kinematically complete breakup geometries: the pp quasi-free-scattering (QFS) configuration, in which the not detected neutron is at rest in the laboratory system, and the space-star (SST) geometry, in which all 3 outgoing nucleons have the same momenta (magnitudes) in the plane which in the 3N c.m. system is perpendicular to the incoming nucleon momentum. The theoretical predictions based on nuclear forces only show, that the cross sections for QFS and SST are quite

stable against changes of the underlying interactions, including also three-nucleon forces [10]. At energies below  $\approx 20$  MeV theory overestimates the SST pd cross sections by  $\approx 10\%$ , and overestimates the pp QFS cross sections by  $\approx 20\%$ , respectively [6, 10]. With increasing energy the theoretical cross sections come close to the data [10], which indicates that the pp Coulomb force is very probably responsible for these low energy discrepancies. However, the Coulomb force effects found in [6] are practically negligible for the pd SST configuration and only slightly improve the description of the pp QFS data [11, 12, 13, 14, 15].

This inability to understand the pp QFS and pd SST cross sections motivated us to reconsider the inclusion of the Coulomb force into momentum space Faddeev calculations. One main concern in such type of calculations is the application of a partial wave decomposition to the long-ranged Coulomb force. Even when screening is applied it seems reasonable to treat from the beginning the screened pp Coulomb t-matrix without partial wave decomposition because the required limit of vanishing screening leads necessarily to a drastic increase of the number of partial wave states involved. As an example we provide numbers for the exponential screening  $e^{-(\frac{r}{R})^n}$ . Taking the screening radius  $R = 20$  fm and  $n = 4$  requires all  $l \leq l_{max} = 10$  partial wave states to reproduce the 3-dimensional pp screened Coulomb t-matrix at  $E_p^{lab} = 13$  MeV. Increasing the screening radius to  $R = 120$  fm requires  $l_{max} \approx 50$  which is a big numerical challenge. Even more, that would lead to an explosion of the number of 3N partial waves required for convergence. Another problem concerns the treatment of the pp Coulomb interaction in its proper coordinate, which is the relative proton-proton distance, throughout the calculations. Any deviation from this restriction can cause effects which are difficult to estimate. Both problems were accounted for in our formulation presented in [9] and applied there to pd elastic scattering.

In the present paper we extend that approach to the pd breakup. Again we apply directly the 3-dimensional screened pp Coulomb t-matrix without relying on a partial wave decomposition. In [9] we demonstrated that the physical pd elastic scattering amplitude can be obtained from the off-shell solutions of the Faddeev equation and has a well defined screening limit. In contrast to elastic scattering, where the amplitude itself does not require renormalisation, in case of the pd breakup the on-shell solutions of the Faddeev equation are required. They demand renormalisation in the screening limit which can be achieved through renormalisation of the pp t-matrices.

In section II for the convenience of the reader we shortly present the main points of the formalism outlined in details in [9]. The screening limit for pd breakup is discussed in section III and the results shown in section IV. The summary is given in section V.

## II. FADDEEV EQUATIONS WITH SCREENED PP COULOMB FORCE

We use the Faddeev equation in the form [10]

$$T|\Phi\rangle = tP|\Phi\rangle + tPG_0T|\Phi\rangle \quad (1)$$

where  $P$  is defined in terms of transposition operators,  $P = P_{12}P_{23} + P_{13}P_{23}$ ,  $G_0$  is the free 3N propagator,  $|\Phi\rangle$  the initial state composed of a deuteron state and a momentum eigenstate of the proton. Knowing  $T|\Phi\rangle$  the breakup as well as the elastic pd scattering amplitudes can be gained by quadratures in the standard manner [10].

We use our standard momentum space partial wave basis  $|pq\tilde{\alpha}\rangle$

$$|pq\tilde{\alpha}\rangle \equiv |pq(ls)j(\lambda\frac{1}{2})I(jI)J(t\frac{1}{2})T\rangle \quad (2)$$

and distinguish between the partial wave states  $|pq\alpha\rangle$  with total 2N angular momentum  $j$  below some value  $j_{max}$ :  $j \leq j_{max}$ , in which the nuclear,  $V_N$ , as well as the pp screened Coulomb interaction,  $V_c^R$  (in isospin  $t = 1$  states only), are acting, and the states  $|pq\beta\rangle$  with  $j > j_{max}$ , for which only  $V_c^R$  is acting in the pp subsystem. The states  $|pq\alpha\rangle$  and  $|pq\beta\rangle$  form a complete system of states

$$\int p^2 dp q^2 dq \sum_{\tilde{\alpha}} |pq\tilde{\alpha}\rangle \langle pq\tilde{\alpha}| = \int p^2 dp q^2 dq \left( \sum_{\alpha} |pq\alpha\rangle \langle pq\alpha| + \sum_{\beta} |pq\beta\rangle \langle pq\beta| \right) = \mathbf{I}. \quad (3)$$

Projecting Eq.(1) for  $T|\Phi\rangle$  on the  $|pq\alpha\rangle$  and  $|pq\beta\rangle$  states one gets the following system of coupled integral equations

$$\begin{aligned} \langle pq\alpha|T|\Phi\rangle &= \langle pq\alpha|t_{N+c}^R P|\Phi\rangle \\ &+ \langle pq\alpha|t_{N+c}^R PG_0 \sum_{\alpha'} \int p'^2 dp' q'^2 dq' |p'q'\alpha'\rangle \langle p'q'\alpha'|T|\Phi\rangle \\ &+ \langle pq\alpha|t_{N+c}^R PG_0 \sum_{\beta'} \int p'^2 dp' q'^2 dq' |p'q'\beta'\rangle \langle p'q'\beta'|T|\Phi\rangle \end{aligned} \quad (4)$$

$$\begin{aligned} \langle pq\beta|T|\Phi\rangle &= \langle pq\beta|t_c^R P|\Phi\rangle \\ &+ \langle pq\beta|t_c^R PG_0 \sum_{\alpha'} \int p'^2 dp' q'^2 dq' |p'q'\alpha'\rangle \langle p'q'\alpha'|T|\Phi\rangle \\ &+ \langle pq\beta|t_c^R PG_0 \sum_{\beta'} \int p'^2 dp' q'^2 dq' |p'q'\beta'\rangle \langle p'q'\beta'|T|\Phi\rangle \end{aligned} \quad (5)$$

where  $t_{N+c}^R$  and  $t_c^R$  are t-matrices generated by the interactions  $V_N + V_c^R$  and  $V_c^R$ , respectively. Namely for states  $|\alpha\rangle$  with two-nucleon subsystem isospin  $t = 1$  the corresponding t-matrix element  $\langle p\alpha|t_{N+c}^R(E - \frac{3}{4m}q^2)|p'\alpha'\rangle$  is a linear combination of the pp,  $t_{pp+c}^R$ , and the neutron-proton (np),  $t_{np}$ ,  $t = 1$  t-matrices, which are generated by the interactions  $V_{pp}^{strong} + V_c^R$  and

$V_{np}^{strong}$ , respectively. The coefficients of that combination depend on the total isospin  $T$  and  $T'$  of states  $|\alpha\rangle$  and  $|\alpha'\rangle$  [9, 16]:

$$\begin{aligned}
\langle t = 1T = \frac{1}{2} | t_{N+c}^R | t' = 1T' = \frac{1}{2} \rangle &= \frac{1}{3} t_{np} + \frac{2}{3} t_{pp+c}^R \\
\langle t = 1T = \frac{3}{2} | t_{N+c}^R | t' = 1T' = \frac{3}{2} \rangle &= \frac{2}{3} t_{np} + \frac{1}{3} t_{pp+c}^R \\
\langle t = 1T = \frac{1}{2} | t_{N+c}^R | t' = 1T' = \frac{3}{2} \rangle &= \frac{\sqrt{2}}{3} (t_{np} - t_{pp+c}^R) \\
\langle t = 1T = \frac{3}{2} | t_{N+c}^R | t' = 1T' = \frac{1}{2} \rangle &= \frac{\sqrt{2}}{3} (t_{np} - t_{pp+c}^R) .
\end{aligned} \tag{6}$$

For isospin  $t = 0$ , in which case  $T = T' = \frac{1}{2}$ :

$$\langle t = 0T = \frac{1}{2} | t_{N+c}^R | t' = 0T' = \frac{1}{2} \rangle = t_{np} . \tag{7}$$

In case of  $t_c^R$  only the screened pp Coulomb force  $V_c^R$  is acting.

The third term on the right hand side of (5) is proportional to  $\langle pq\beta | t_c^R PG_0 | p'q'\beta' \rangle \langle p'q'\beta' | t_c^R$ . A direct calculation of its isospin part shows that independently from the value of the total isospin  $T$  it vanishes [9].

Inserting  $\langle pq\beta | T | \Phi \rangle$  from (5) into (4) one gets

$$\begin{aligned}
\langle pq\alpha | T | \Phi \rangle &= \langle pq\alpha | t_{N+c}^R P | \Phi \rangle + \langle pq\alpha | t_{N+c}^R PG_0 t_c^R P | \Phi \rangle \\
&- \langle pq\alpha | t_{N+c}^R PG_0 \sum_{\alpha'} \int p'^2 dp' q'^2 dq' | p'q'\alpha' \rangle \langle p'q'\alpha' | t_c^R P | \Phi \rangle \\
&+ \langle pq\alpha | t_{N+c}^R PG_0 \sum_{\alpha'} \int p'^2 dp' q'^2 dq' | p'q'\alpha' \rangle \langle p'q'\alpha' | T | \Phi \rangle \\
&+ \langle pq\alpha | t_{N+c}^R PG_0 t_c^R PG_0 \sum_{\alpha'} \int p'^2 dp' q'^2 dq' | p'q'\alpha' \rangle \langle p'q'\alpha' | T | \Phi \rangle \\
&- \langle pq\alpha | t_{N+c}^R PG_0 \sum_{\alpha'} \int p'^2 dp' q'^2 dq' | p'q'\alpha' \rangle \langle p'q'\alpha' | t_c^R PG_0 \\
&\quad \sum_{\alpha''} \int p''^2 dp'' q''^2 dq'' | p''q''\alpha'' \rangle \langle p''q''\alpha'' | T | \Phi \rangle .
\end{aligned} \tag{8}$$

This is a coupled set of integral equations in the space of the states  $|\alpha\rangle$  only, which incorporates the contributions of the pp Coulomb interaction from all partial wave states up to infinity. It can be solved by iteration and Pade summation [9, 10].

When compared to our standard treatment without screened Coulomb force [10] there are two new leading terms  $\langle pq\alpha | t_{N+c}^R PG_0 t_c^R P | \Phi \rangle$  and  $-\langle pq\alpha | t_{N+c}^R PG_0 | \alpha' \rangle \langle \alpha' | t_c^R P | \Phi \rangle$ . The first term must be calculated using directly the 3-dimensional screened Coulomb t-matrix  $t_c^R$ , while the second term requires partial wave projected screened Coulomb t-matrix elements in the  $|\alpha\rangle$  channels only. The kernel also contains two new terms. The term  $\langle pq\alpha | t_{N+c}^R PG_0 t_c^R PG_0 | \alpha' \rangle \langle$

$\alpha'|T|\Phi\rangle$  must again be calculated with a 3-dimensional screened Coulomb t-matrix while the second one,  $\langle pq\alpha|t_{N+c}^R PG_0|\alpha'\rangle \langle \alpha'|t_c^R PG_0|\alpha''\rangle \langle \alpha''|T|\Phi\rangle$ , involves only the partial wave projected screened Coulomb t-matrix elements in the  $|\alpha\rangle$  channels. The calculation of the new terms with the partial wave projected Coulomb t-matrices follows our standard procedure. Namely the two sub kernels  $t_{N+c}^R PG_0$  and  $t_c^R PG_0$  are applied consecutively on the corresponding state. The detailed expressions how to calculate the new terms with the 3-dimensional screened Coulomb t-matrix are given in Appendix A of Ref. [9].

The transition amplitude for breakup  $\langle \Phi_0|U_0|\Phi\rangle$  is given in terms of  $T|\Phi\rangle$  by [10, 17]

$$\langle \Phi_0|U_0|\Phi\rangle = \langle \Phi_0|(1+P)T|\Phi\rangle \quad (9)$$

where  $|\Phi_0\rangle = |\vec{p}\vec{q}m_1m_2m_3\nu_1\nu_2\nu_3\rangle$  is the free state. The permutations acting in momentum-, spin-, and isospin-spaces can be applied to the bra-state  $\langle \phi_0| = \langle \vec{p}\vec{q}m_1m_2m_3\nu_1\nu_2\nu_3|$  changing the sequence of nucleons spin and isospin magnetic quantum numbers  $m_i$  and  $\nu_i$  and leading to well known linear combinations of the Jacobi momenta  $\vec{p}, \vec{q}$ . Thus evaluating (9) it is sufficient to regard the general amplitudes  $\langle \vec{p}\vec{q}m_1m_2m_3\nu_1\nu_2\nu_3|T|\Phi\rangle \equiv \langle \vec{p}\vec{q}|T|\Phi\rangle$ . Using Eq. (1) and the completeness relation (3) one gets:

$$\begin{aligned} \langle \vec{p}\vec{q}|T|\Phi\rangle &= \langle \vec{p}\vec{q}|\sum_{\alpha'} \int p'^2 dp' q'^2 dq' |p'q'\alpha'\rangle \langle p'q'\alpha'|T|\Phi\rangle \\ &- \langle \vec{p}\vec{q}|\sum_{\alpha'} \int p'^2 dp' q'^2 dq' |p'q'\alpha'\rangle \langle p'q'\alpha'|t_c^R P|\Phi\rangle \\ &- \langle \vec{p}\vec{q}|\sum_{\alpha'} \int p'^2 dp' q'^2 dq' |p'q'\alpha'\rangle \langle p'q'\alpha'|t_c^R PG_0 \sum_{\alpha''} \int p''^2 dp'' q''^2 dq'' |p''q''\alpha''\rangle \langle p''q''\alpha''|T|\Phi\rangle \\ &+ \langle \vec{p}\vec{q}|t_c^R P|\Phi\rangle + \langle \vec{p}\vec{q}|t_c^R PG_0 \sum_{\alpha'} \int p'^2 dp' q'^2 dq' |p'q'\alpha'\rangle \langle p'q'\alpha'|T|\Phi\rangle . \end{aligned} \quad (10)$$

It follows, that in addition to the amplitudes  $\langle pq\alpha|T|\Phi\rangle$  also the partial wave projected amplitudes  $\langle pq\alpha|t_c^R P|\Phi\rangle$  and  $\langle pq\alpha|t_c^R PG_0|\alpha'\rangle \langle \alpha'|T|\Phi\rangle$  are required. The expressions for the contributions of these three terms to the transition amplitude for the breakup reaction are given in Appendix B of Ref. [9].

The last two terms in (10) again must be calculated using directly 3-dimensional screened Coulomb t-matrices. In Appendix C of Ref. [9] the expression for  $\langle \vec{p}\vec{q}|t_c^R P|\Phi\rangle$  and in Appendix D of Ref. [9] the last matrix element  $\langle \vec{p}\vec{q}|t_c^R PG_0|\alpha'\rangle \langle \alpha'|T|\Phi\rangle$  are given.

### III. THE SCREENING LIMIT

The set of coupled Faddeev equations (8) is well defined for any finite screening radius. It is an exact set assuming that the strong NN t-matrix can be neglected beyond a certain  $j_{max}$ , which is justified. Further the pp screened Coulomb force is taken into account to infinite order in the partial wave decomposition in form of the 3-dimensional screened Coulomb t-matrix  $t_{pp}^{cR}$ . The important challenge is to control the screening limit for the physical pd breakup amplitude (9). In case of elastic scattering we provided in Ref. [9] analytical arguments and showed numerically that the physical elastic pd scattering amplitude itself has a well defined screening limit and does not require renormalisation. This can be traced back to the fact that to get the elastic pd scattering amplitude it is sufficient to solve the Faddeev equations (8) for off-shell values of the Jacobi momenta

$$\frac{p^2}{m} + \frac{3}{4m}q^2 \neq E . \quad (11)$$

The off-shell Faddeev amplitudes  $\langle pq\alpha | T | \Phi \rangle$  of Eq.(8) are determined by off-shell nucleon-nucleon t-matrix elements  $t(p, p'; E - \frac{3}{4m}q^2)$ , which have a well defined screening limit (see the following discussion and examples).

Contrary to pd elastic scattering the physical breakup amplitude (9) corresponds to the on-shell values of Jacobi momenta

$$\frac{p^2}{m} + \frac{3}{4m}q^2 = E \equiv \frac{3}{4m}q_{max}^2 . \quad (12)$$

That means that the physical pd breakup amplitude (10) requires on-shell Faddeev amplitudes  $\langle p_0q\alpha | T | \Phi \rangle$  together with the four, also on-shell, additional terms in (8), with  $p_0 = \sqrt{\frac{3}{4}(q_{max}^2 - q^2)}$ . The on-shell Faddeev amplitudes can be obtained from the off-shell solutions  $\langle pq\alpha | T | \Phi \rangle$  using (8):

$$\begin{aligned} \langle p_0q\alpha | T | \Phi \rangle &= \langle p_0q\alpha | t_{N+c}^R P | \Phi \rangle + \langle p_0q\alpha | t_{N+c}^R P G_0 t_c^R P | \Phi \rangle \\ &- \langle p_0q\alpha | t_{N+c}^R P G_0 \sum_{\alpha'} \int p'^2 dp' q'^2 dq' | p'q'\alpha' \rangle \langle p'q'\alpha' | t_c^R P | \Phi \rangle \\ &+ \langle p_0q\alpha | t_{N+c}^R P G_0 \sum_{\alpha'} \int p'^2 dp' q'^2 dq' | p'q'\alpha' \rangle \langle p'q'\alpha' | T | \Phi \rangle \\ &+ \langle p_0q\alpha | t_{N+c}^R P G_0 t_c^R P G_0 \sum_{\alpha'} \int p'^2 dp' q'^2 dq' | p'q'\alpha' \rangle \langle p'q'\alpha' | T | \Phi \rangle \\ &- \langle p_0q\alpha | t_{N+c}^R P G_0 \sum_{\alpha'} \int p'^2 dp' q'^2 dq' | p'q'\alpha' \rangle \langle p'q'\alpha' | t_c^R P G_0 \\ &\quad \sum_{\alpha''} \int p''^2 dp'' q''^2 dq'' | p''q''\alpha'' \rangle \langle p''q''\alpha'' | T | \Phi \rangle . \end{aligned} \quad (13)$$

These on-shell amplitudes together with additional, also on-shell, terms in (10) define the physical breakup amplitude (9). That in consequence requires half-shell t-matrix elements  $t(p_0, p'; \frac{p_0^2}{m})$  which

are of 3 types: the partial wave projected pure screened Coulomb  $t_c^R$  generated by  $V_c^R$ , the partial wave projected  $t_{N+c}^R$  generated by  $V_{strong} + V_c^R$ , and the 3-dimensional screened Coulomb matrix elements.

It is well known [1, 18, 19] that in the screening limit  $R \rightarrow \infty$  such half-shell t-matrices acquire an infinitely oscillating phase factor  $e^{i\Phi_R(p)}$ , where  $\Phi_R(p)$  depends on the type of the screening. For the exponential screening its form depends on two parameters, the screening radius  $R$  and the power  $n$ :

$$V_c^R(r) = \frac{\alpha}{r} e^{-(\frac{r}{R})^n} . \quad (14)$$

At a given value  $n$  the pure Coulomb potential results for  $R \rightarrow \infty$ . As has been shown in [20] based on [21, 22], the related phase  $\Phi_R(p)$  is given as

$$\Phi_R(p) = -\eta[\ln(2pR) - \epsilon/n] \quad (15)$$

where  $\epsilon = 0.5772\dots$  is the Euler number and  $\eta = \frac{m_p \alpha}{2p}$  the Sommerfeld parameter.

Contrary to the half-shell, the off-shell t-matrix elements do not acquire such an oscillating phase and their screening limit is well defined.

In Figs. 1-3 we demonstrate that behavior for the 3-dimensional half-shell screened Coulomb pp t-matrix [23]. Increasing the screening radius  $R$  changes drastically the imaginary part of the t-matrix (Fig. 2a). The real part is more stable but does not approach the pure Coulomb limit (Fig. 1a). Renormalizing by the phase factor  $e^{-i\Phi_R(p)}$  of Eq. (15) provides a well defined limit to the pure Coulomb half-shell result of Ref. [24] (Fig. 1b and 2b).

For the 3-dimensional off-shell screened Coulomb pp t-matrix the pure Coulomb screening limit of Ref. [25, 26] is achieved without any renormalisation factor for screening radii  $R > 20$  fm (Fig. 3).

Analogous behavior for the partial wave decomposed  $l = 0$  half-shell screened Coulomb  $t_c^R$  and the  ${}^1S_0$   $t_{pp+c}^R$  t-matrices is shown in Figs. 4 and 5, respectively. While the imaginary part again exhibits drastic changes when the screening radius increases (Fig. 4a and 5a), removing the phase factor  $e^{-i\Phi_R(p)}$  (renormalisation) provides a well defined limit for the screening radii  $R > 40$  fm (Fig. 4b and 5b). It is seen that in case when the screened Coulomb potential is combined with the strong force also the real part of the half-shell t-matrix undergoes strong changes with increased screening (Fig. 5a).

For the partial wave decomposed off-shell  $l = 0$  screened Coulomb  $t_c^R$  and the  ${}^1S_0$   $t_{pp+c}^R$  t-matrix elements a well defined screening limit is reached without any renormalisation (Fig. 6b and 6a, respectively).

That oscillatory phase factor appearing in the half-shell proton-proton t-matrices requires a careful treatment of (13) to get the screening limit for the  $\langle p_0 q \alpha | T | \Phi \rangle$  amplitudes. Namely for the states  $|\alpha\rangle$  with the two-nucleon subsystem isospin  $t = 1$  the corresponding t-matrix element  $\langle p_0 \alpha | t_{N+c}^R(\frac{p_0^2}{m}) | p' \alpha' \rangle$  is a linear combination of the pp and neutron-proton (np)  $t = 1$  t-matrices, the coefficients of which depend on the total isospin  $T$  and  $T'$  of the states  $|\alpha\rangle$  and  $|\alpha'\rangle$  (see discussion after (5)). It follows that to achieve the screening limit one needs to renormalize the pp t-matrix  $t_{pp+c}^R$  in that combination before performing the action of the operators in (13). The term in that linear combination coming with the np t-matrix  $t_{np}$  does not require renormalisation.

#### IV. NUMERICAL RESULTS

To demonstrate the feasibility of our approach we applied the outlined formalism to a simple dynamical model in which the nucleon-nucleon force was restricted to act in  $^1S_0$  and  $^3S_1 - ^3D_1$  partial waves only and taken from the CD Bonn potential [27]. The proton-proton Coulomb force was modified by the exponential screening (14) with the screening radius  $R$  and  $n = 1$ .

To investigate the screening limit  $R \rightarrow \infty$  we generated set of partial-wave decomposed t-matrices,  $t_c^R$ , based on the screened pp Coulomb force only or combined with the strong pp interaction,  $t_{pp+c}^R$ , taking  $R = 20, 40, 60, 80, 100, 120$  and  $140$  fm. With that dynamical input we solved the set of Faddeev equations (8) for off-shell values of the Jacobi momenta  $p$  and  $q$  and for the total angular momenta of the p-p-n system up to  $J \leq \frac{15}{2}$  and both parities. Then the on-shell Faddeev amplitudes  $\langle p_0 q \alpha | T | \Phi \rangle$  were gained through (13). In this first study we restricted ourselves to the perturbative approximation for the 3-dimensional screened Coulomb t-matrix:  $t_c^R = V_c^R$ . Of course in the future studies that approximation will be avoided and the full solution of the 3-dimensional LS equation for the screened pp Coulomb t-matrix will be used [23]. When calculating observables we also omitted the last term  $\langle \Phi_0 | (1 + P) t_c^R P G_0 T | \Phi \rangle$  in (10) coming with the 3-dimensional screened Coulomb t-matrix.

The results for the breakup reaction are shown in Figs. 7-10 where the exclusive cross sections  $\frac{d^5\sigma}{d\Omega_1 d\Omega_2 dS}$  for the QFS and SST configurations parametrized through the arc-length of the kinematical S-curve are presented.

For the QFS and SST (see Fig. 7 and 9, respectively) the convergence in the screening radius is achieved at  $R = 60$  fm. For QFS the Coulomb force decreases the cross section with respect to the nd case and brings the theory close to the pd data. For SST the Coulomb force also brings theory close to the pd data, however, only at S-values close to the space-star condition ( $S \approx 6$  MeV). For

S-values further away the theory is far above the pd data.

The theoretical prediction for both geometries results through interference of different terms contributing to the breakup amplitude. The importance and magnitudes of the contributions coming from different terms in the breakup amplitude differs for those two geometries (see Fig. 8 and Fig. 10). In both cases the largest is the contribution of the first term in (10)  $\langle \Phi_0 | (1 + P) | \alpha \rangle \langle \alpha | T | \Phi \rangle$  (black dashed-dotted line in Figs. 8 and 10). For QFS and SST the cross section resulting from that term is below the pd data and below the full result which encompasses all terms (solid line). The magnitudes of three additional terms:  $\langle \Phi_0 | (1 + P) t_c^R P | \Phi \rangle$  (the fourth term in (10) calculated with the 3-dimensional screened Coulomb t-matrix, here approximated by  $V_c^R$ , and given by the green short-dashed line), the second term in (10)  $\langle \Phi_0 | (1 + P) | \alpha \rangle \langle \alpha | t_c^R P | \Phi \rangle$  (calculated with the partial-wave projected screened Coulomb t-matrix and given by the blue dashed-double-dotted line), and the third term in (10)  $\langle \Phi_0 | (1 + P) | \alpha \rangle \langle \alpha | t_c^R P G_0 T | \Phi \rangle$  (calculated again with the partial-wave projected screened Coulomb t-matrix and given by the maroon double-dashed-dotted line), are small. Because they are difficult to see on the scale of Figs. 8a and Fig. 10a they are again presented in the part b) of these figures. For both configurations the term with the 3-dimensional t-matrix  $\langle \Phi_0 | (1 + P) t_c^R P | \Phi \rangle$  gives the smallest contribution. Smallness of these terms does not mean however, that they are unimportant because the interference effects are nonnegligible and act in different ways for QFS and SST.

For the QFS the second largest contribution comes from  $\langle \Phi_0 | (1 + P) | \alpha \rangle \langle \alpha | t_c^R P | \Phi \rangle$  (blue dashed-double-dotted line) while for SST it comes from  $\langle \Phi_0 | (1 + P) | \alpha \rangle \langle \alpha | t_c^R P G_0 T | \Phi \rangle$  (maroon double-dashed-dotted line). For QFS and SST taking the amplitude of that second largest contribution together with  $\langle \Phi_0 | (1 + P) | \alpha \rangle \langle \alpha | T | \Phi \rangle$  changes significantly the cross section. For QFS it is the black dotted line in Fig. 8a resulting from  $\langle \Phi_0 | (1 + P) | \alpha \rangle \langle \alpha | (T - t_c^R P) | \Phi \rangle$  while for SST it is blue long-dashed line in Fig. 10a resulting from  $\langle \Phi_0 | (1 + P) | \alpha \rangle \langle \alpha | (T - t_c^R P G_0 T) | \Phi \rangle$ .

The third largest contribution provides for both configurations smaller changes of the cross section and the result when the second and third largest contributions are included  $\langle \Phi_0 | (1 + P) | \alpha \rangle \langle \alpha | (T - t_c^R P G_0 T - t_c^R P) | \Phi \rangle$  is given by the red long-dashed line. It is above the pd data for both geometries.

Finally, including the smallest contribution from the 3-dimensional screened Coulomb t-matrix  $\langle \Phi_0 | (1 + P) t_c^R P | \Phi \rangle$  brings the theory to the pd data for the QFS geometry at all S-values and for the SST configuration at S-values close to the space-star condition.

## V. SUMMARY AND CONCLUSIONS

We extended our approach to include the pp Coulomb force into the momentum space 3N Faddeev calculations presented in Ref. [9] for elastic scattering to the pd breakup. It is based on a standard formulation for short range forces and relies on the screening of the long-range Coulomb interaction. In order to avoid all uncertainties connected with the application of the partial wave expansion, unsuitable when working with long-range forces, we apply directly the 3-dimensional pp screened Coulomb t-matrix.

Using a simple dynamical model for the nuclear part of the interaction we demonstrated feasibility of that approach for the treatment of the pd breakup. We demonstrated that contrary to the pd elastic scattering, where the resulting amplitudes do not require renormalisation, it is unavoidable to perform renormalisation of the pp half-shell t-matrices in order to get the physical breakup amplitude. Namely that amplitude has two contributions, one driven by the interaction in the pp subsystem and second in the np subsystem. Only the first part requires renormalisation.

We have shown that converged results for breakup can be achieved with finite screening radii.

We calculated contributions of different terms to the breakup cross section in QFS and SST configurations. The interference between different contributions leads to an interference pattern, which is different for QFS and SST configurations. In our restricted dynamical model the pp Coulomb interaction brings the nd breakup cross sections close to the pd data for the QFS configuration. Also for the SST geometry in the vicinity of the space-star condition the pd theory is close to the pd data. However, further away on the S-curve the theory lies above the data.

In future studies the perturbative approximation for the 3-dimensional screened Coulomb t-matrix will be avoided and higher partial wave components of the nucleon-nucleon interaction will be included.

### Acknowledgments

This work was supported by the Polish 2008-2011 science funds as a research project No. N N202 077435. It was also partially supported by the Helmholtz Association through funds provided to the virtual institute “Spin and strong QCD”(VH-VI-231) and by the European Community-Research Infrastructure Integrating Activity “Study of Strongly Interacting Matter” (acronym HadronPhysics2, Grant Agreement n. 227431) under the Seventh Framework Programme of EU. The numerical calculations have been performed on the supercomputer cluster of the JSC, Jülich,

Germany.

---

- [1] E. O. Alt, W. Sandhas, and H. Ziegelmann, Phys. Rev. **C 17**, 1981 (1978).
- [2] E. O. Alt and W. Sandhas, in Coulomb Interactions in Nuclear and Atomic Few-Body Collisions, ed. by F.S. Levin and D. Micha (Plenum, New York 1996), p.1.
- [3] E. O. Alt and M. Rauh, Phys. Rev. **C49**, R2285 (1994).
- [4] E. O. Alt, A. M. Mukhamedzhanov, M. M. Nishonov, and A. I. Sattarov, Phys. Rev. **C65**, 064613 (2002).
- [5] A. Kievsky, M. Viviani, and S. Rosati, Phys. Rev. **C 52**, R15 (1995).
- [6] A. Deltuva, A. C. Fonseca, and P. U. Sauer, Phys. Rev. **C72**, 054004 (2005).
- [7] A. Deltuva, A. C. Fonseca, and P. U. Sauer, Phys. Rev. **C71**, 054005 (2005).
- [8] E. Stephan et al., Phys. Rev. **C76**, 057001 (2007).
- [9] H. Witała, R. Skibiński, J. Golak, W. Glöckle, nucl-th 0903.1522v2.
- [10] W. Glöckle, H. Witała, D. Hüber, H. Kamada, J. Golak, Phys. Rep. **274**, 107 (1996).
- [11] G. Rauprich et al., Nucl. Phys. **A535**, 313 (1991).
- [12] R. Großmann et al., Nucl. Phys. **A603**, 161 (1996).
- [13] H. Patberg et al., Phys. Rev. **C53**, 1497 (1996).
- [14] M. Allet et al., Few-Body Syst. **C20**, 27 (1996).
- [15] J. Zejma et al., Phys. Rev. **C55**, 42 (1997).
- [16] H. Witała, W. Glöckle, H.Kamada, Phys. Rev. **C43**,1619 (1991).
- [17] W. Glöckle, The Quantum Mechanical Few-Body Problem, Springer Verlag 1983.
- [18] W.F. Ford, Phys. Rev. **133**, B1616 (1964).
- [19] W.F. Ford, J. Math. Phys. **7**, 626 (1966).
- [20] M. Yamaguchi, H. Kamada, and Y. Koike, Prog. Theor. Phys. **114** , 1323 (2005).
- [21] J.R. Taylor, Nuovo Cimento **B23**, 313 (1974).
- [22] M.D. Semon and J.R. Taylor, Nuovo Cimento **A26**, 48 (1975).
- [23] R. Skibiński, J. Golak, H. Witała, and W.Glöckle, Eur. Phys. J. **A40**, 215 (2009).
- [24] L.P. Kok and H. van Haeringen, Phys. Rev. Lett. **46**, 1257 (1981).
- [25] J.C.Y. Chen and A.C. Chen, in Advances of Atomic and Molecular Physics, edited by D. R. Bates and J. Estermann ( Academic, New York, 1972), Vol. 8.
- [26] L.P. Kok and H. van Haeringen, Phys. Rev. **C21**, 512 (1980).
- [27] R. Machleidt, F. Sammarruca, and Y. Song, Phys. Rev. **C53**, R1483 (1996).
- [28] H. R. Setze et al., Phys. Rev. **C71**, 034006 (2005).

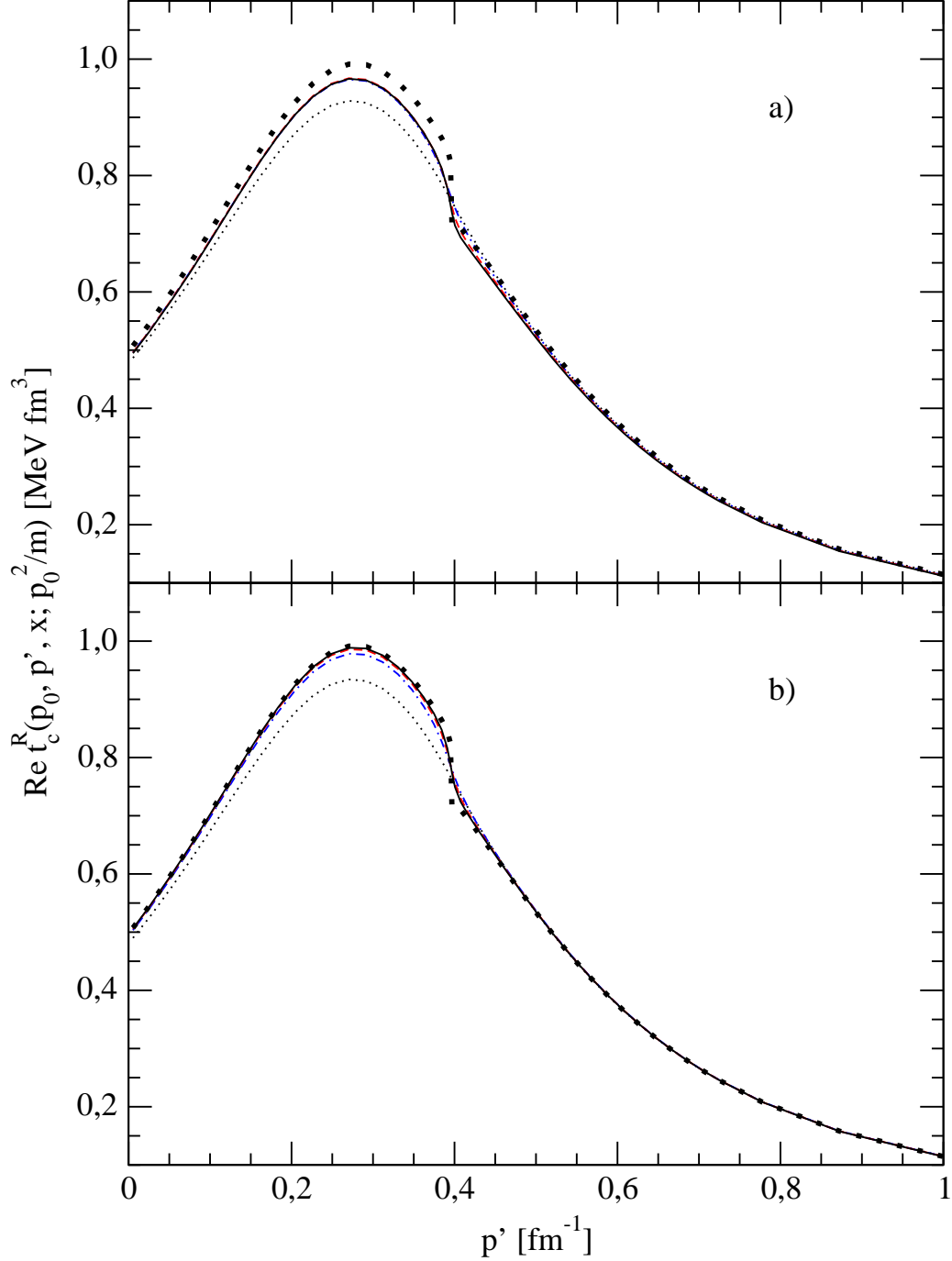


FIG. 1: (color online) The real part of the nonrenormalized (a) and renormalized (b) 3-dimensional half-shell screened Coulomb pp t-matrix  $t_c^R(p_0, p', x; \frac{p_0^2}{m})$ . The lines correspond to the exponential screening with  $n = 1$  and different screening radii:  $R = 20$  fm (black dotted line),  $R = 60$  fm (blue dashed-dotted line),  $R = 120$  fm (red dashed line),  $R = 180$  fm (black solid line). The Coulomb half-shell result of Ref. [24] is given by thick dots. The momentum  $p_0 = 0.396 \text{ fm}^{-1}$  and  $x = 0.706$ .

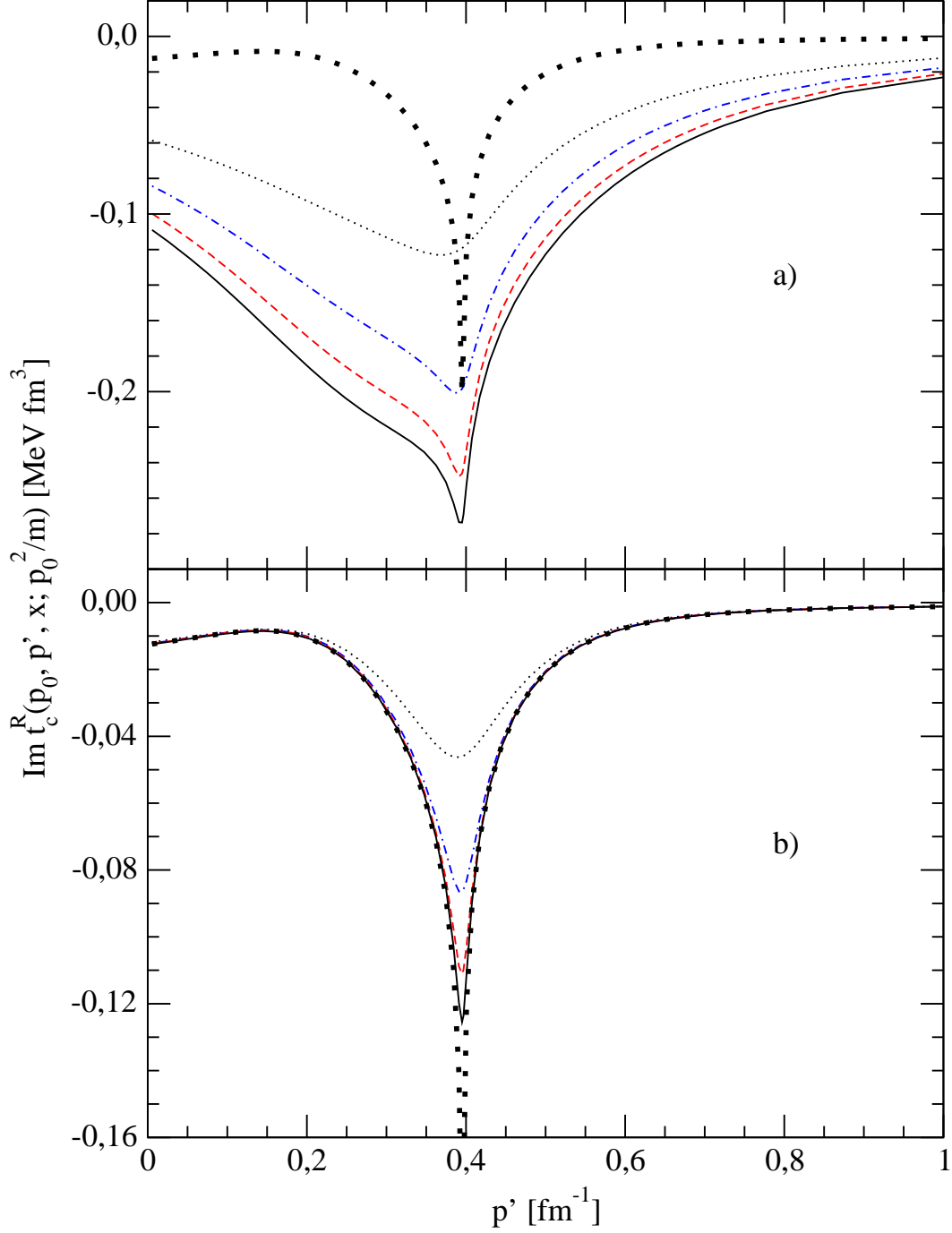


FIG. 2: (color online) The imaginary part of the nonrenormalized (a) and renormalized (b) 3-dimensional half-shell screened Coulomb pp t-matrix  $t_c^R(p_0, p', x; \frac{p_0^2}{m})$ . For the description of the lines and values of  $p_0$  and  $x$  see Fig. 1.

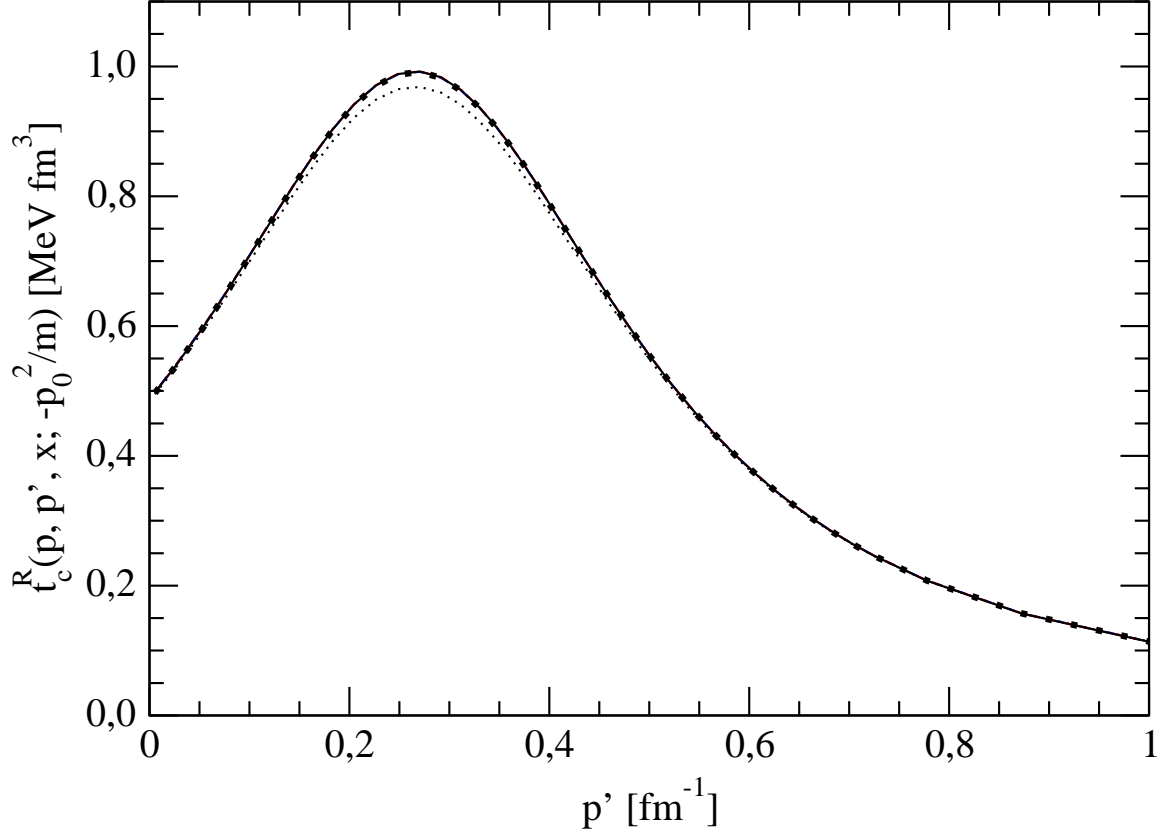


FIG. 3: (color online) The 3-dimensional off-shell screened Coulomb pp t-matrix  $t_c^R(p, p', x; -\frac{p_0^2}{m})$ . The lines correspond to the exponential screening with  $n = 1$  and different screening radii:  $R = 20$  fm (black dotted line),  $R = 60$  fm (blue dashed-dotted line),  $R = 120$  fm (red dashed line),  $R = 180$  fm (black solid line). The Coulomb off-shell result of Ref. [25, 26] is given by thick dots. The momentum  $p_0 = 0.396$  fm $^{-1}$ ,  $p = 0.375$  fm $^{-1}$  and  $x = 0.706$ .

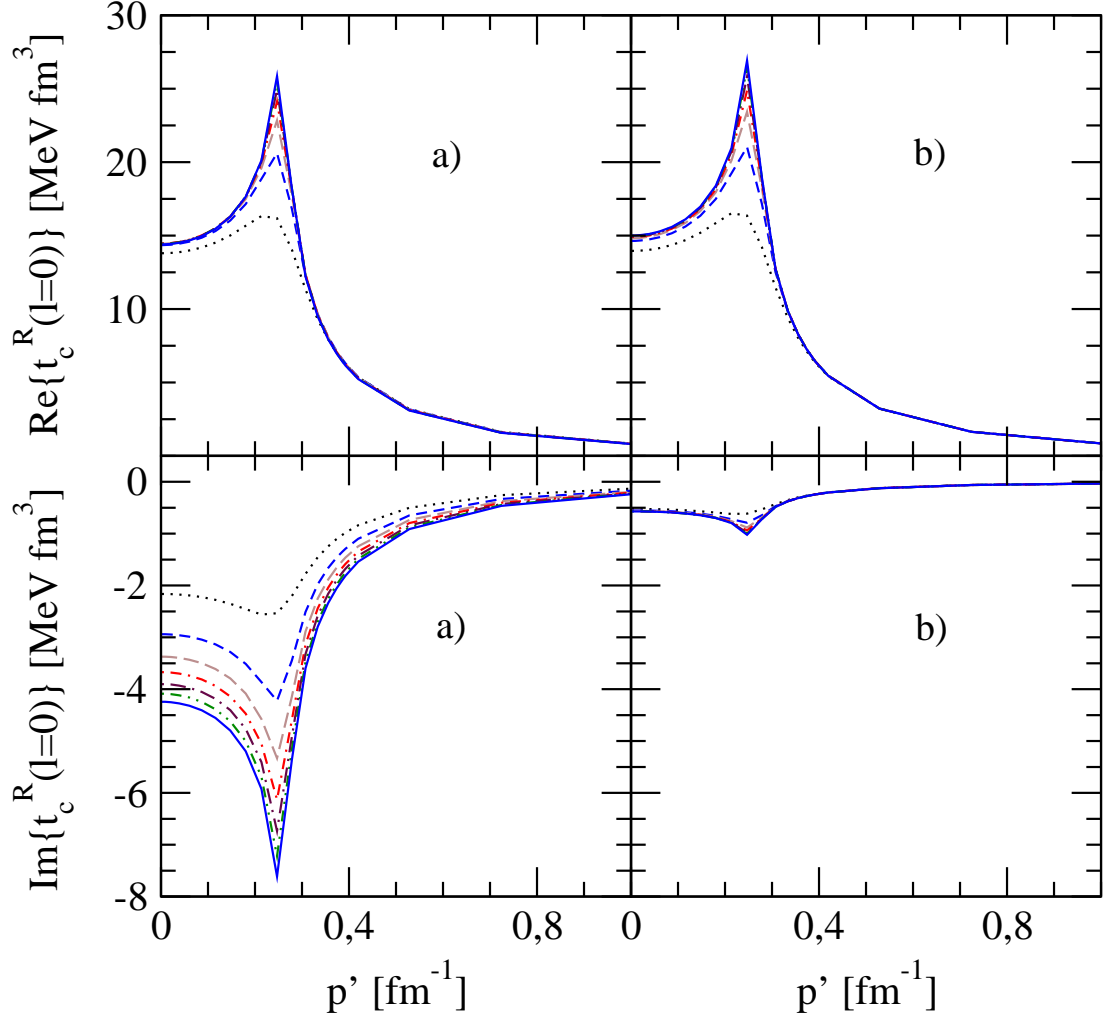


FIG. 4: (color online) The real (upper panels) and imaginary (lower panels) parts of the nonrenormalized (a) and renormalized (b)  $l = 0$  half-shell screened Coulomb pp t-matrix  $t_c^R(p_0, p', \frac{p_0^2}{m})$ . The lines correspond to the exponential screening with  $n = 1$  and different screening radii:  $R = 20$  fm (black dotted line),  $R = 40$  fm (blue short-dashed line),  $R = 60$  fm (brown long-dashed line),  $R = 80$  fm (red short-dashed-dotted line),  $R = 100$  fm (maroon long-dashed-dotted line),  $R = 120$  fm (green short-dashed-double-dotted line),  $R = 140$  fm (blue solid line). The momentum  $p_0 = 0.26 \text{ fm}^{-1}$ .

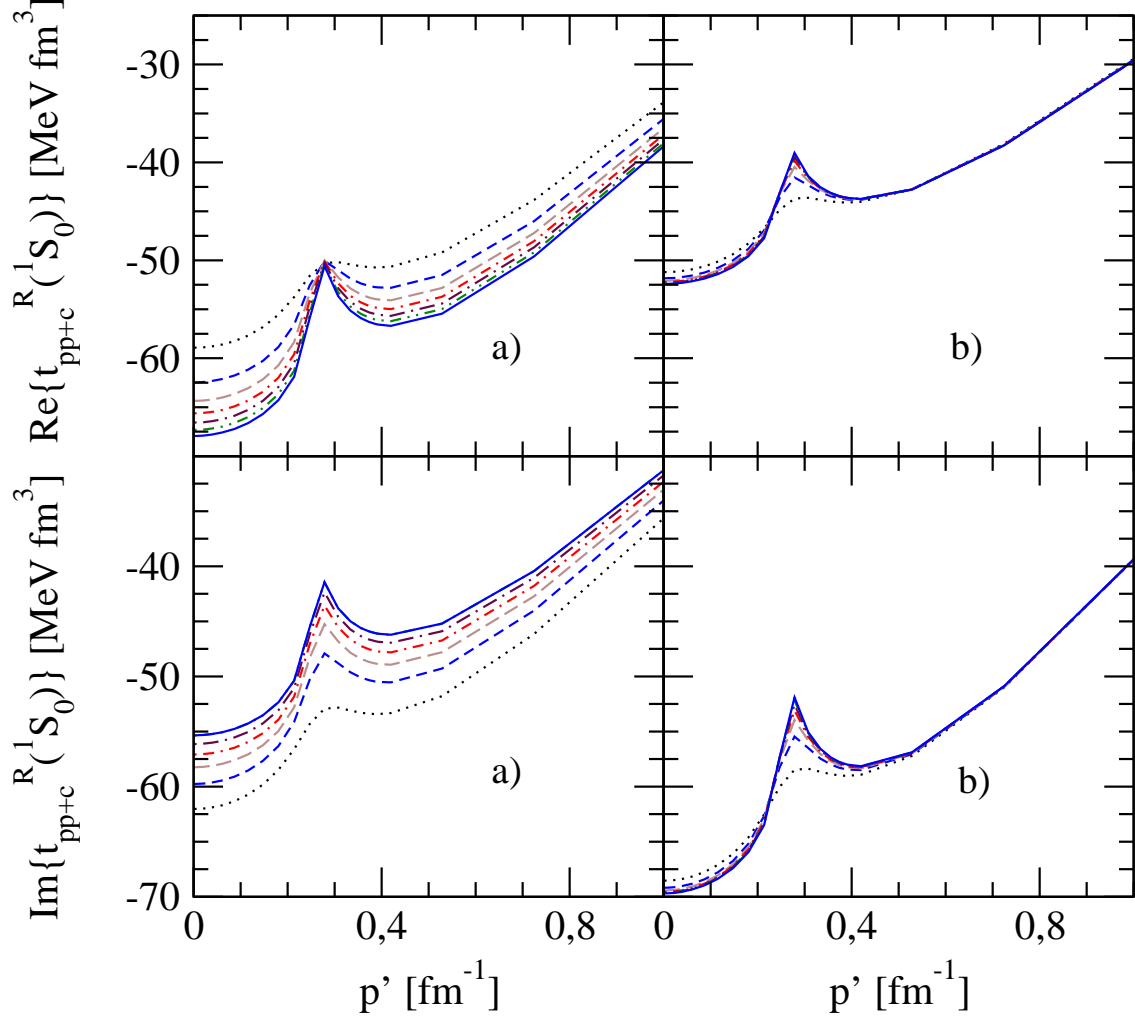


FIG. 5: (color online) The real (upper panels) and imaginary (lower panels) parts of the nonrenormalized (a) and renormalized (b)  $^1S_0$  half-shell pp t-matrix  $t_{pp+c}^R(p_0, p', \frac{p_0^2}{m})$ . The lines correspond to the exponential screening with  $n = 1$  and different screening radii:  $R = 20$  fm (black dotted line),  $R = 40$  fm (blue short-dashed line),  $R = 60$  fm (brown long-dashed line),  $R = 80$  fm (red short-dashed-dotted line),  $R = 100$  fm (maroon long-dashed-dotted line),  $R = 120$  fm (green short-dashed-double-dotted line),  $R = 140$  fm (blue solid line). The momentum  $p_0 = 0.26 \text{ fm}^{-1}$ .

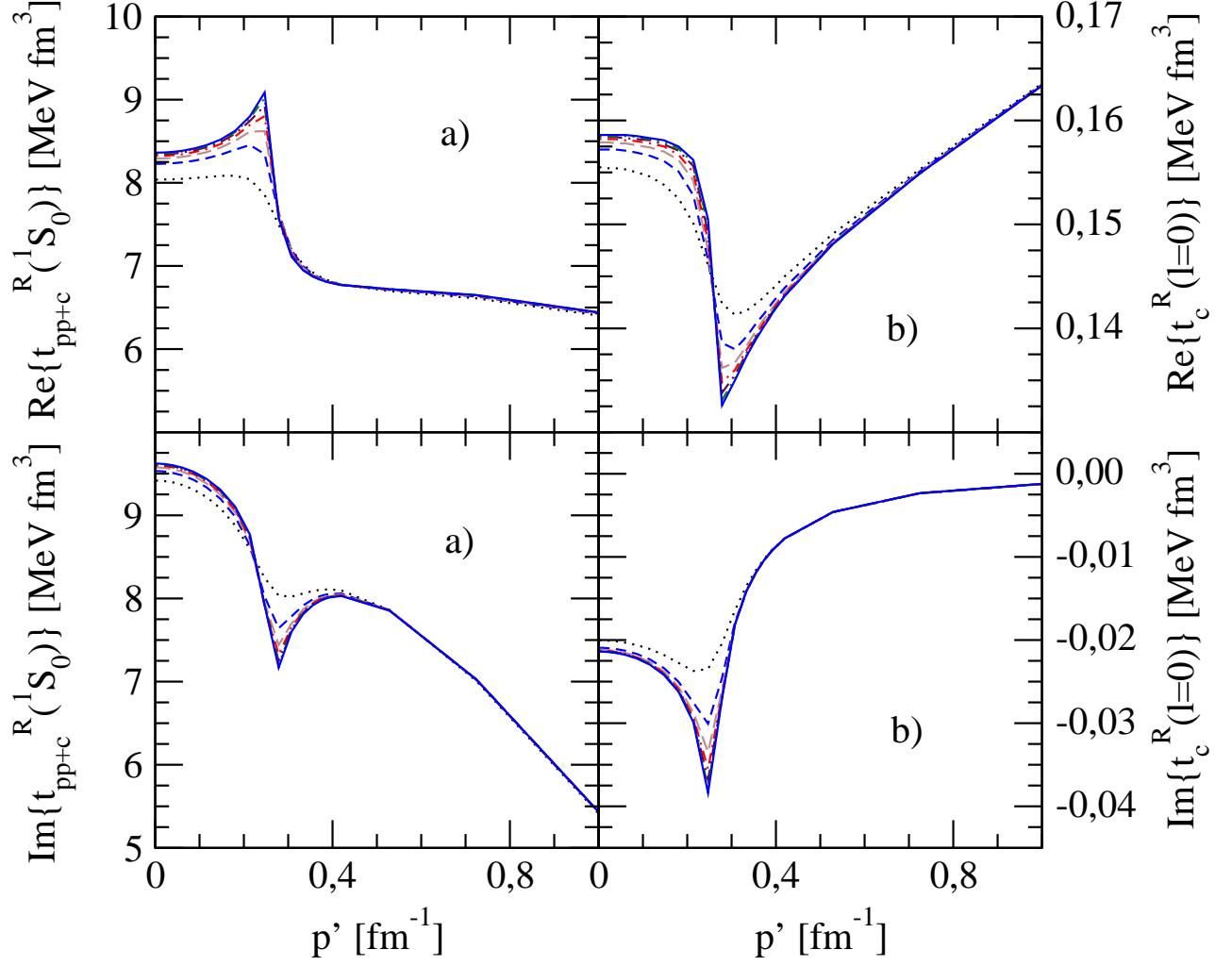


FIG. 6: (color online) The real (upper panels) and imaginary (lower panels) parts of the  ${}^1S_0 t_{pp+c}^R(p, p', \frac{p_0^2}{m})$  (a) and the  $l = 0$  screened Coulomb  $t_c^R(p, p', \frac{p_0^2}{m})$  (b) off-shell t-matrices. For the description of the lines see Fig. 4. The momentum  $p_0 = 0.26 \text{ fm}^{-1}$  and  $p = 2.38 \text{ fm}^{-1}$ .

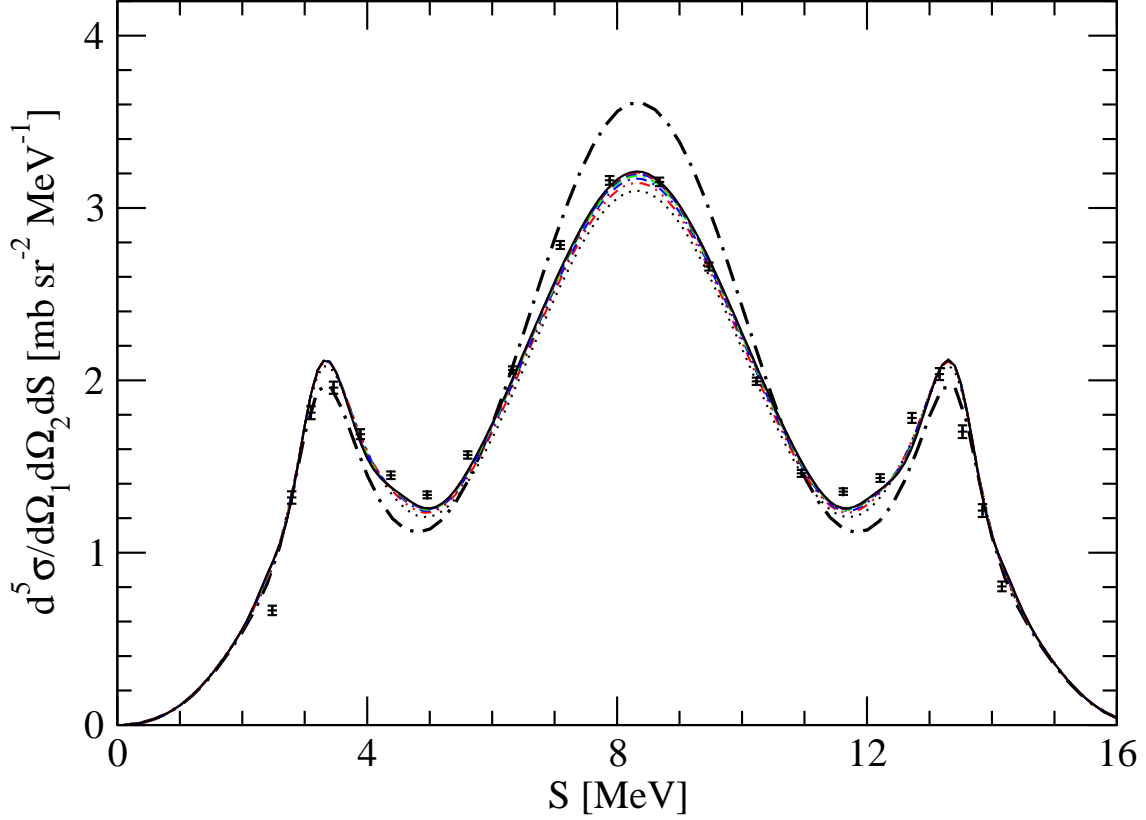


FIG. 7: (color online) The convergence in the cut-off radius  $R$  of the  $d(p, p_1 p_2)n$  breakup cross section in a kinematically complete QFS configuration with polar angles of the two outgoing protons  $\theta_1 = \theta_2 = 39^\circ$  and azimuthal angle  $\phi_{12} = 180^\circ$ . The incoming proton energy is  $E_p^{lab} = 13$  MeV and theoretical predictions are based on a screened Coulomb force and the CD Bonn nucleon-nucleon potential [27] restricted to  $^1S_0$  and  $^3S_1$ - $^3D_1$  partial waves. The screening radius is:  $R = 20$  fm (black dotted line),  $R = 40$  fm (green dashed-double-dotted line),  $R = 60$  fm (blue dashed-dotted line),  $R = 80$  fm (red double-dashed-dotted line),  $R = 100$  fm (blue dashed line),  $R = 120$  fm (red long-dashed line),  $R = 140$  fm (black solid line). The black long-dashed-dotted line is the break-up cross section with the pp Coulomb interaction switched-off. The pluses are  $E_p^{lab} = 13$  MeV pd breakup data of Ref. [11].

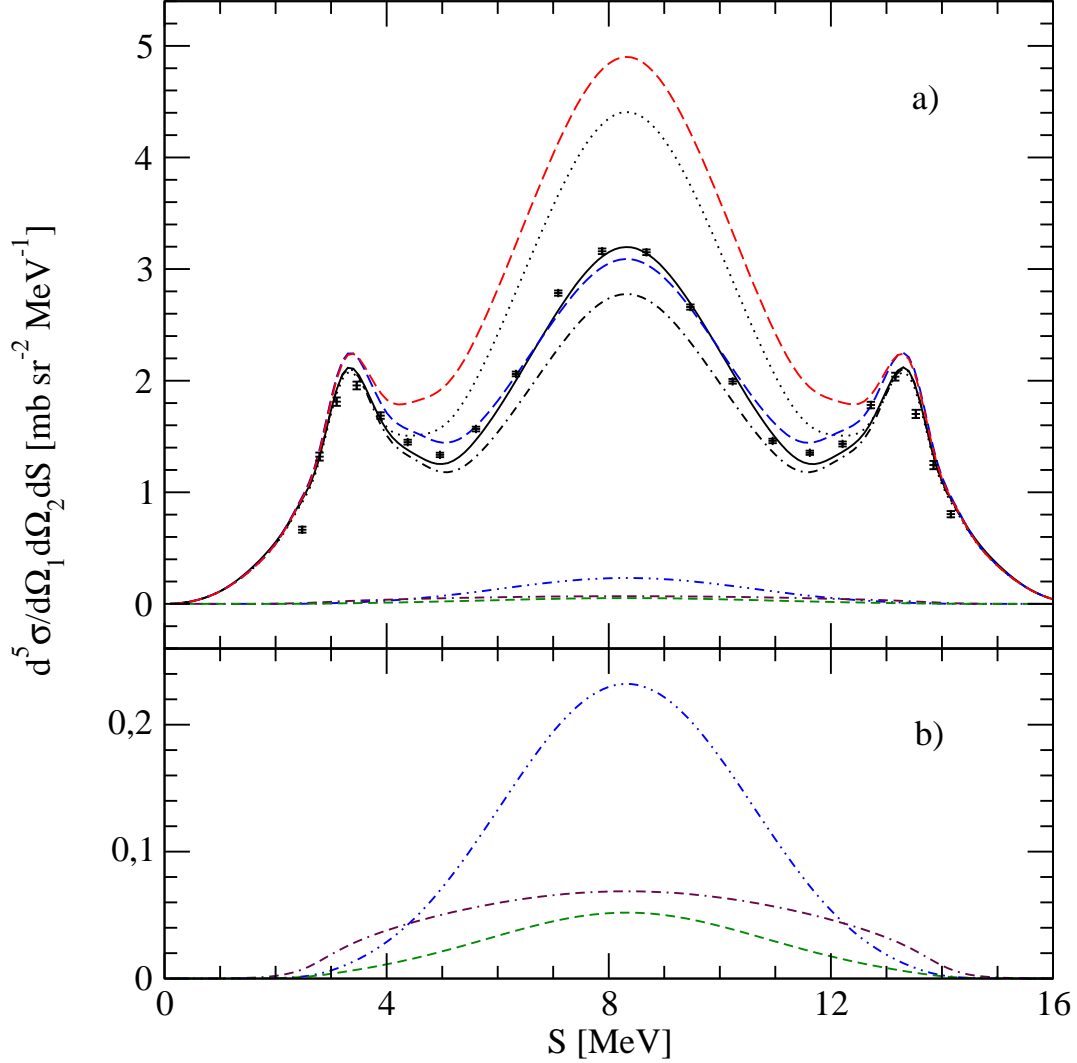


FIG. 8: (color online) In part a): the contribution of different terms to the cross section of the QFS configuration of Fig. 7. The (black) dashed-dotted line is the contribution of the first term  $\langle \Phi_0 | (1+P) | \alpha \rangle \langle \alpha | T | \Phi \rangle$  in (10) and the (green) short-dashed line is the contribution of the fourth term  $\langle \Phi_0 | (1+P) t_c^R P | \Phi \rangle$  in (10) coming with the 3-dimensional screened Coulomb t-matrix  $t_c^R$  (in the present calculation  $t_c^R = V_c^R$ ). The (blue) dashed-double-dotted and (maroon) double-dashed-dotted lines are contributions of the second  $\langle \Phi_0 | (1+P) | \alpha \rangle \langle \alpha | t_c^R P | \Phi \rangle$  and of the third  $\langle \Phi_0 | (1+P) | \alpha \rangle \langle \alpha | t_c^R P G_0 T | \Phi \rangle$  term in (10), respectively, which are calculated with partial-wave decomposed screened Coulomb t-matrix. The (black) dotted and (blue) long-dashed lines result from the  $\langle \Phi_0 | (1+P) | \alpha \rangle \langle \alpha | (T - t_c^R P) | \Phi \rangle$  and  $\langle \Phi_0 | (1+P) | \alpha \rangle \langle \alpha | (T - t_c^R P G_0 T) | \Phi \rangle$  amplitudes, respectively. The (red) long-dashed line is the contribution of the  $\langle \Phi_0 | (1+P) | \alpha \rangle \langle \alpha | (T - t_c^R P - t_c^R P G_0 T) | \Phi \rangle$  amplitude. The (black) solid line encompasses all four terms. All results are for screening radius  $R = 100$  fm. The part b) of the figure shows contributions of small terms which are difficult to see on the scale of part a).

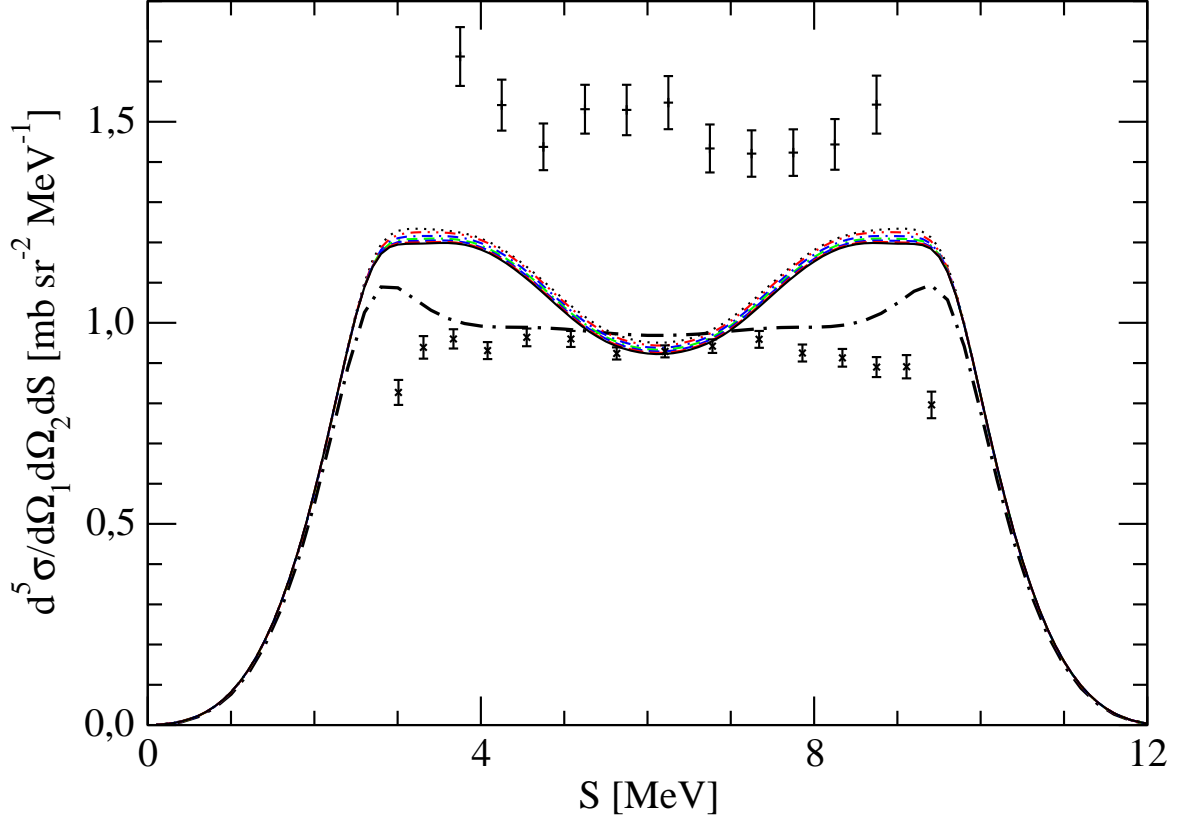


FIG. 9: (color online) The convergence in the cut-off radius  $R$  of the  $d(p, p_1 p_2)n$  breakup cross section in a kinematically complete SST configuration with polar angles of the two outgoing protons  $\theta_1 = \theta_2 = 50.5^\circ$  and azimuthal angle  $\phi_{12} = 120^\circ$ . The incoming proton energy is  $E_p^{lab} = 13$  MeV and the theoretical predictions are based on the screened Coulomb force and the CD Bonn nucleon-nucleon potential [27] restricted to  $^1S_0$  and  $^3S_1$ - $^3D_1$  partial waves. For the description of the lines see Fig. 7. The x-es are  $E_p^{lab} = 13$  MeV pd breakup data of Ref. [11] and pluses are  $E_n^{lab} = 13$  MeV nd breakup data of Ref. [28].

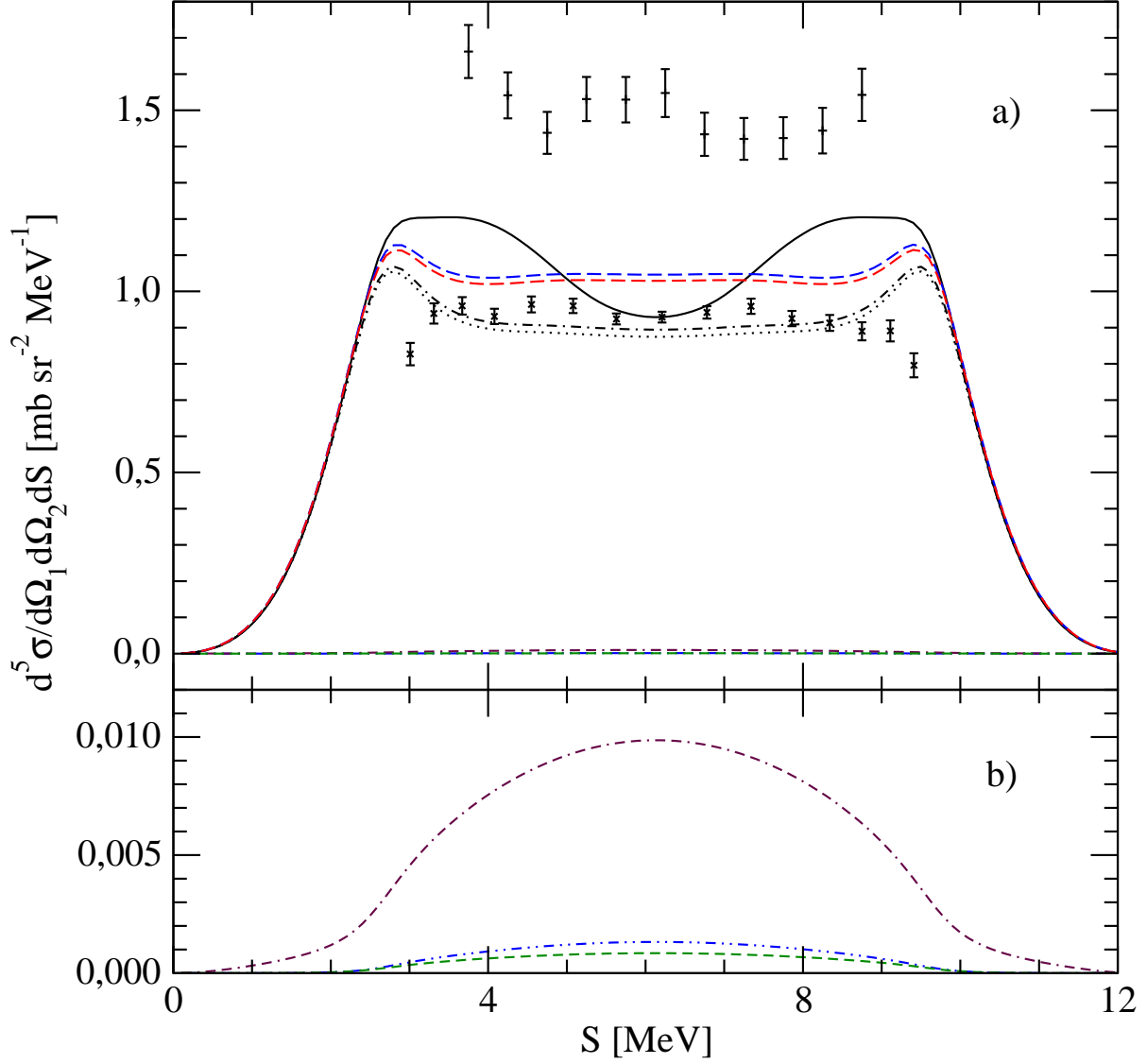


FIG. 10: (color online) In part a): the contribution of different terms to the cross section of the SST configuration of Fig. 9. The solid line encompasses all terms. For the description of other lines see Fig. 8. All results are for screening radius  $R = 100$  fm. The part b) of the figure shows contributions of small terms which are difficult to see on the scale of part a).